Research Article

Characterization of Polyvinylpyrrolidone-2-Acrylamide-2-Methlypropansulphonic Acid Based Polymer as a Corrosion Inhibitor for Copper and Brass in Hydrochloric Acid

Mamookho Elizabeth Makhatha, George M. Tsoeunyane and Luyanda Masana Yvette Maqubela
Department of Engineering Metallurgy, University of Johannesburg, Johannesburg, 2028, South Africa

Sergei Sherbakov and Daria Podgayskaya
Joint Institute of Mechanical Engineering of the National Academy of Sciences of Belarus, 220072, Minsk, Belarus

Vishwanatha H. M.*
Department of Mechanical and Industrial Engineering, Manipal Institute of Technology, Manipal Academy of Higher Education, Manipal, 576104, Karnataka, India

Pawan Kumar*
Department of Engineering Metallurgy, University of Johannesburg, Johannesburg, 2028, South Africa
Joint Institute of Mechanical Engineering of the National Academy of Sciences of Belarus, 220072, Minsk, Belarus

* Corresponding author. E-mail: vishwanatha.hm@manipal.edu, kumarpawan@mail.ru
DOI: 10.14416/j.asep.2024.07.013
Received: 9 May 2024; Revised: 14 June 2024; Accepted: 28 June 2024; Published online: 26 July 2024

Abstract
Copper and its alloy are susceptible to corrosion in heat exchangers during acid cleaning. The corrosion leads to materials loss and damage; hence it is important to prohibit such corrosion damage using an eco-friendly corrosion inhibitor. In the current work, a polymer composite-based corrosion inhibitor was prepared using polyvinylpyrrolidone (PVP) and 2-Acrylamido-2-methylpropane sulfonic acid (AMPS). The PVP copolymer undergoes polymerization with the AMPS having several interconnected uniformly sized pores and produces a PVP–AMPS composite with rod-like microstructure. The effect of concentration, time, and temperature on corrosion inhibition efficiency (IE) of PVP–AMPS composite was studied for copper and brass in hydrochloric acid (HCl) solution. The IE increases with concentration and decreases with time and temperature. A change in cathodic and anodic Tafel slopes with the concentration of PVP–AMPS inhibitors was observed. The increase in IE with concentration was attributed to the solubility of PVP–AMPS composite in HCl. However, the decrease in IR with time and temperature was due to the desorption of PVP–AMPS composite from the surface of copper and brass and also due to the exothermic reactions at higher temperature. A few peaks in FTIR spectra at 3000–3100 cm^{-1} were missing, which is due to the stretching vibration of H–C during the crosslinking polymerization. Further, the absence of the O–H peak indicated that the polymerization process removed the water molecule. The best correlation coefficient (R^2) for the Langmuir adsorption mechanism was achieved. A negative Gibbs free energy (ΔG) envisages the spontaneity of the adsorption process. However, the $|\Delta G|$ for adsorption was less than 20 $kJmol^{-1}$ confirming the process as physisorption. A shift in anodic and cathodic branches in the presence of the PVP–AMPS inhibitor indicated a mixed-type inhibitor behavior.

Keywords: Clean technology, Corrosion inhibition, Mixed-type inhibitor, Polymer composite

1 Introduction

Copper corrosion has been reported to be a problem that is difficult to treat in heat exchangers due to scale formation produced during the operation of systems [1]. Such problems in treating result in decreased performance of heat exchangers and unprompted stoppages. Therefore, the need arises for pickling, cleaning, and descaling of the acid layers to enhance the performance [2], [3]. Studies have shown that corrosion is of great concern in the gas and oil industries as 25% of the total losses experienced in such industries are due to corrosion and these losses in cost for billions of dollars per year [4].

Corrosion inhibitors are used to protect the base metals from deterioration and to ensure the removal of scale during acid cleaning [5]–[7]. The inhibitors during the interaction decrease the rate of attack in the given corrosion environment and are of great importance in the pipeline industries [8]–[11]. The inhibition property is due to the presence of N, S, and P in organic compounds, the heteroatoms [12]. These heteroatoms catalyze the functionality of the absorption processes and thereby enhance the inhibition activity. Due to the higher adsorption capacity of the organic compounds on the given metal surface, they are considered efficient and successful inhibitors [13]. The monomer 2-acrylamide-2-methylpropane sulphonic acid (AMPS) is widely preferred in water treatment because of its thermal and anti-hydrolytic stability. During the application, it is found that the AMPS can easily become an auto polymer/copolymer and hence can perform favorably [14]. The molecular structure of AMPS greatly influences the corrosion inhibition due to adsorption. The structure of AMPS consisting of an adequate number of electron-donating functional groups attached to the structure favors adsorption. Hence, the AMPS undergoes adsorption onto the wide area of the copper surface resulting in enhanced inhibition efficiency [15].

In the acidizing industrial processes, inhibitors are mixed with the acidic solutions. The hyper effects of acids on the liners, casting materials, and tubes are reduced by the use of inhibitors. So, proper selection of corrosion inhibitors plays a vital role in industrial applications. In the recent past, there has been tremendous attention to green and eco-friendly inhibitors. Among these are polyvinyl pyrrolidone (PVP), poly ethylenimine, and caffeic acid have been of great interest [16]. The PVP is a synthetic polymer, which sustainable, eco-friendly, water-soluble, low toxic, and possesses good— adhesion, emulsification, and physiological compatibility. PVP is a typical organic corrosion inhibitor generally preferred in acidic environments. It is found to be an effective metal corrosion inhibitor [17], [18].

In recent times, polymer composites-based corrosion inhibitors have been of great interest. Such inhibitors, due to the metal chelation process form the inhibition layer in the corrosive environments. Hence, they perform actively. The majority of the acidic inhibitors are activity-specific and are target-based for a specific application. The blending of polymer inhibitors may result in combined effects of corrosion inhibition. Further, such blends may also result in a convenient addition of the homopolymer characteristics. Such combos are non-linear in the majority of compositions and hence might result in improved characteristics. Therefore, the proper choice of blends of polymers plays a crucial role in gaining enhanced inhibition characteristics [19]. There have several studies reported on blended polymers used as corrosion inhibitors [20]–[22]. However, there exists little literature on PVP-based polymer blended composite as corrosion inhibitors for industrial applications. With the aim to establish improved eco-friendly polymer composites, the current work focuses on the utilization of polymer composites as corrosion inhibitors for copper and copper alloys in an acidic medium. In this regard, the current work introduces the synthesis of a PVP–AMPS polymer composite-based corrosion inhibitor and tests the inhibition efficiency against copper and brass samples in an acidic medium.

2 Materials and Methodology

2.1 *Synthesis of the PVP–AMPS composite*

The PVP–AMPS polymer composite is synthesized using Polyvinylpyrrolidone (PVP) and 2-Acrylamide-2-Methlypropansulphonic acid (AMPS) compounds. The structures of the raw materials are shown in Figure 1.

The PVP–AMPS copolymer corrosion inhibitor was synthesized by solution polymerization where 10% of PVP and 5% of AMPS solution in 1 M of oxalic acid were mixed. The mixture was further stirred for 2 h in freshly prepared 1% ammonium per sulfate maintained at 0–5 °C in an ice water bath. During stirring, ammonium hydroxide was added to maintain the pH between 6–8. Further, a non-solvent liquid (acetone) was added to allow precipitation, and

the entire mixture was refrigerated for 24 h to form the PVP–AMPS copolymer. The formed composite was precipitated out, filtered, washed, and air-dried. The PVP–AMPS copolymer was characterized using FTIR to confirm polymerization and by XRD for phase identification. Then, the copolymer was subjected to corrosion testing. The current work is exhibited as per the workflow diagram shown in Figure 2. More details about the solution polymerization have been reported elsewhere [23], [24].

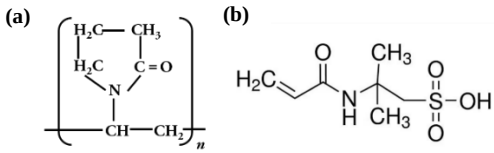

Figure 1: Structure of (a) PVP and (b) AMPS.

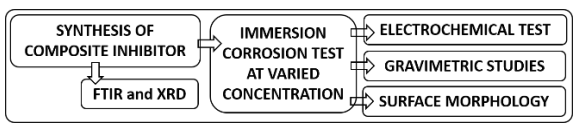

Figure 2: Workflow diagram.

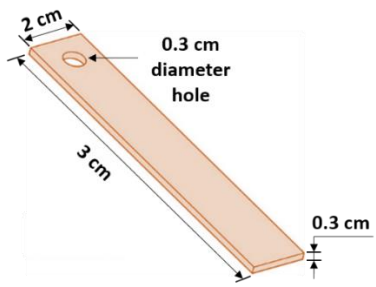

Figure 3: Schematic of the coupon.

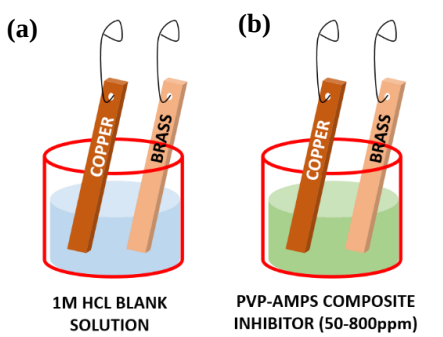

Figure 4: Schematic of immersion of copper and brass coupons in (a) blank solution and (b) PVP–AMPS composite solution.

2.2 *Test materials*

Copper and brass coupons were used as the test materials. The schematic of the coupons is shown in Figure 3. The dimensions (L × B × t) of the coupons were (3 × 2 × 0.3) cm. The coupons were drilled with a 0.3 cm diameter hole for easy handling of coupons during immersion in the corrosion medium. All coupons were engraved for easy identification. The coupons were prepared using standard metallography sample preparation techniques. The samples were ground using 600–1200 grit sandpaper followed by cleaning in acetone and drying using a dryer. The coupons were subjected to gravimetric studies, electrochemical analysis, and surface analysis. Then, the samples were subjected to corrosion testing in two different solutions, a blank solution and the PVP–AMPS copolymer solution. A 1M HCl blank solution, an acidic corrosion medium, was prepared by using the industrially used 32% HCl solution. The concentration of the PVP–AMPS inhibitor was varied from 50–800 ppm.

2.3 *Testing and characterization*

A weight loss test was conducted on the samples. The copper and brass coupons were immersed in 1M HCl blank solution and also in the PVP–AMPS inhibitor as shown in Figure 4, at varied concentrations of PVP–AMPS.

For optimization of the concentration of the inhibitor, each immersion was carried out for 3 h. Time plays a very crucial role in the analysis of the efficiency of the corrosion inhibitor. To study the firmness of the film formed by the inhibitor and the adsorption rate of the inhibitor, the immersion test was conducted at fixed time intervals of 3, 9, 12, and 24 h. To analyze the corrosion behavior and mechanisms involved, the following factors were considered: corrosion rate (CR) in $mg.cm^{-2}h^{-1}$, inhibition efficiency (IE), and surface coverage (θ). The CR was estimated using Equation (1).

$$CR = \frac{87.6W}{ADt} \quad (1)$$

where W (g) is the weight loss of the copper and brass, a (cm^2) is the exposed area, D (g/cm^3) is the density, and t (h) is the immersion time. The IE was estimated using Equation (2).

$$IE = \frac{CR_0 - CR_{in}}{CR_0} \times 100 \quad (2)$$

where IE is the inhibition efficiency, CR_0 and CR_{in} represent the corrosion rates of copper and brass coupons estimated without and with the inhibitor respectively. The surface coverage was estimated using Equation (3).

$$\theta = \frac{IE}{100} \quad (3)$$

The process was repeated for other factors such as the effect of immersion time and temperature for an hour. The thermodynamics, as well as the kinetics of the adsorption of the inhibitor, were obtained as a function of temperature. The inhibitory mechanism of PVP–AMPS inhibitor was estimated through the electrochemical studies conducted using an electrochemical analyzer (SP-150 Bio-Logic ASA Potentiostat) fitted with a data acquisition facility (EC-Lab software). Initially, to determine the room temperature steady-state potential of the copper and brass coupons, the coupons were exposed to an open circuit potential *vs* Ag/AgCl for about 30 min. Later, a 3-electrode electrochemical cell was used for electrochemical measurements. The cell consisted of a) reference made up of Ag/AgCl, b) counter electrode made up of graphite rod, and c) working electrodes made up of coupons of copper or brass. During the measurements, an area of 1cm^2 of the copper and brass coupons was immersed in the cell. At a potential range of −250 to +250 mV, the potentiodynamic polarization curves were determined at a scan rate of 5 mVs^{-1}. The obtained polarization data was analyzed in an electrochemical software to determine the corrosion current density (I_{corr}), corrosion potential (E_{corr}), and the Tafel plots. Later, IE was calculated using Equation (4). The experiments were repeated twice to confirm the repeatability.

$$IE = \frac{I_{corr(blank\ HCl)} - I_{corr\ (PVP-AMPS)}}{I_{corr\ (PVP-AMPS)}} \quad (4)$$

Where the $I_{corr\ (blank)}$ and $I_{corr\ (inhibitor)}$ indicate the current densities with the absence and presence of PVP–AMPS inhibitor, respectively. The Tafel parameters (β_a and β_c) and the corrosion current I_{corr} were estimated by extrapolation techniques. Further, the VASP technique was applied to calculate polarization resistance [12]. The correlation between the impedance data and the equivalent circuit was established [25]. For the frequency of 100 kHz to 100 mHz, a sinus amplitude of 5 mV was applied to both copper and brass. Finally, Nyquist plots were used to represent the charge transfer resistance and determine the inhibition efficiencies.

The surface morphology of the copper and brass coupons after the immersion test was analyzed using a scanning electron microscope (TESCAN VEGA 3).

3 Results and Discussion

3.1 *Characterization of PVP–AMPS*

FTIR analysis was carried out to confirm the polymerization between PVP and AMPS. In solution polymerization of PVP and AMPS, AMPS is attached to the PVP matrix through the carbonyl and sulphonate group to form a grafted polymer. The attached APMS increases the electron density on the PVP polymer matrix. The PVP forms a linear backbone of the copolymer while the AMPS is randomly distributed along the backbone. The FTIR spectrum of the PVP–AMPS polymer copolymer inhibitor is shown in Figure 5.

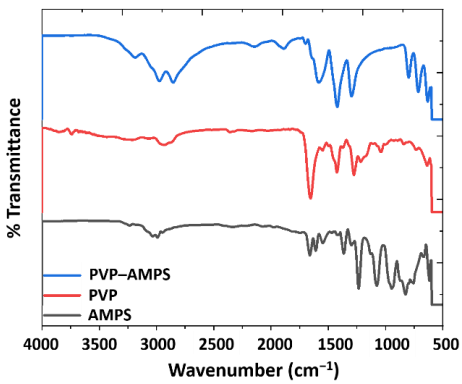

Figure 5: FTIR Spectra of PVP–AMPS inhibitor, AMPS, and PVP.

The peaks for PVP at 2927 and 1655.41 cm^{-1} indicate the existence of symmetric and asymmetric stretching of CH_2 and C=O. The C–H bending and CH_2 wagging are observed at 1425 cm^{-1} and 1276 cm^{-1}, respectively. The peaks at 1041 cm^{-1} and 637 cm^{-1} are identified as the CH_2 rock and N–C=O bending, respectively. The absorption bands for AMPS observed at 3236.35 cm^{-1} and 2992 cm^{-1} are due to the N–H and C–H stretching bands, respectively. The characteristic band of AMPS observed at 1076.91 cm^{-1} is the SO group. The C=O and the secondary amide N–H deformation peak of

AMPS are observed at 1661.49 cm^{-1} and 1548.57 cm^{-1}, respectively. Similar observations are also reported in the literature [26]–[28].

The observed band for PVP–AMPS inhibitor at 3187.34 cm^{-1} is attributed to the N–H stretching of AMPS and PVP. The methyl and methylene vibration bands are observed at 2855.78 cm^{-1}. The vibrational stretching of the sulphonic acid of AMPS is observed at a peak of 1297.14 cm^{-1}. The peaks of PVP–AMPS at 1699.23 cm^{-1} and 1421.80.14 cm^{-1} represent the HNC–O and C–N of amide groups for AMPS and PVP respectively. The disappearance of the peaks at 3000–3100 cm^{-1} is possibly due to the stretching vibration of HC during the crosslinking polymerization of AMPS [29]. It appears that due to the removal of the water molecule during the process of polymerization, the O-H peak is not observed in the composite. The observed band stretches from the FTIR indicate the decreased peak intensity and slight peak shifting from the usually observed positions. This phenomenon is caused by the decreased electron density that is due to the grafting of AMPS on the backbone of the PVP polymer matrix [30].

The SEM images of AMPS, PVP, and PVP–AMPS composite are shown in Figure 6. The SEM image of AMPS shown in Figure 6(a) consists of several interconnected uniformly sized pores. The SEM image of the PVP copolymer shown in Figure 6(b) consists of nearly spherical-shaped large-sized particles. The structure of the binary mixture of PVP–AMPS composite shown in Figure 6(c) consists of rod-like structures [31]. The peak position in Figure 7(b) and (c) appear at different 2Θ degree angles; moreover, the intensity count in Figure 7(b) has decreased as compared to Figure 7(c), suggesting that the amorphous phase in PVP was involved with the crystalline phase in AMPS to form PVP–AMPS copolymer [32]. Further, the XRD analysis of the constituents was also carried out to identify the phases formed as a result of polymerization.

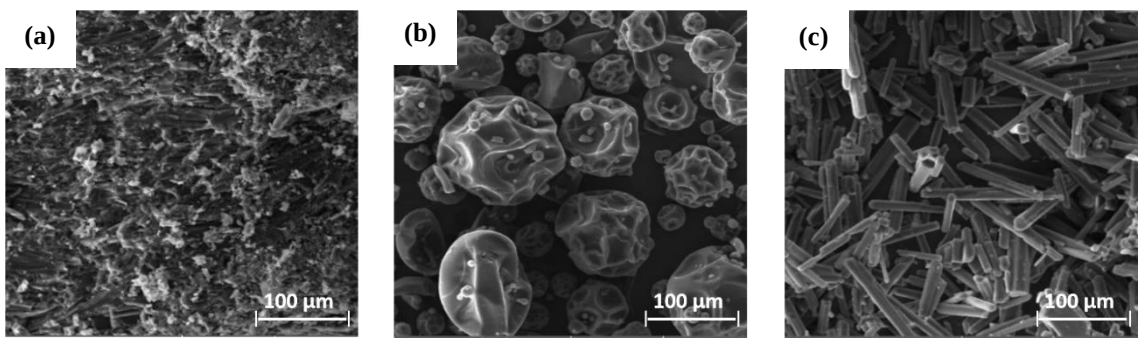

Figure 6: SEM images of (a) AMPS, (b) PVP, and (c) PVP–AMPS composite.

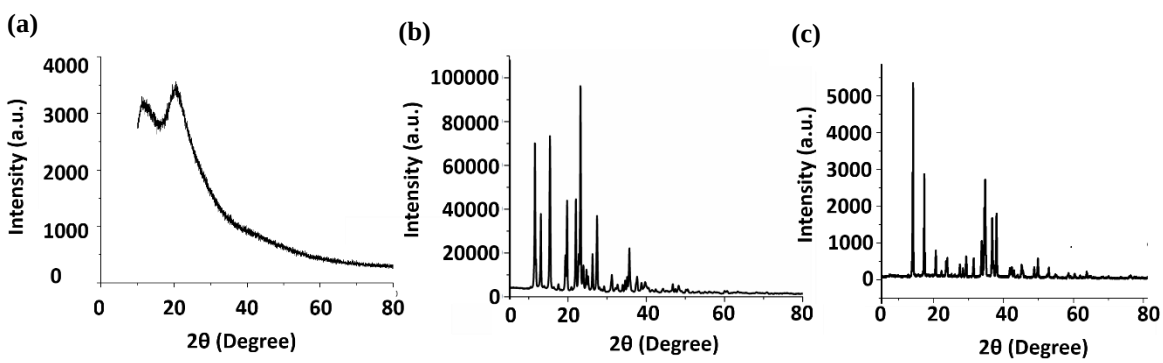

Figure 7: XRD patterns for (a) PVP, (b) AMPS, and (c) PVP–AMPS composite.

The XRD patterns of the copolymer (PVP), the monomer (AMPS), and the polymer composite (PVP–AMPS) are shown in Figure 7(a)–(c). The XRD pattern for PVP shows two broad peaks indicating an amorphous structure with the presence of fewer sharp peaks as compared to that of AMPS and PVP–AMPS.

The XRD patterns of AMPS and PVP–AMPS consist of several peaks indicating crystallinity. The XRD pattern of PVP–AMPS in Figure 7(c) is completely different from that of PVP which confirms the occurrence of the process of polymerization. The crystallinity of the polymer composite makes the inhibitor water soluble [33].

3.2 *Gravimetric studies*

3.2.1 Effect of concentration

The results of the weight loss tests conducted by varying the concentration of the PVP–AMPS show that the corrosion rate decreases with the increase in the concentration of PVP–AMPS. This indicates that there is an increase in the inhibition efficiency (IE) with the concentration of PVP–AMPS inhibitor and the increase is attributed to the solubility of PVP–AMPS in the corrosive media [34]. At 800 ppm of PVP–AMPS inhibitor, the highest IE is obtained and is attributed to the presence of N and O elements in the PVP–AMPS polymer composite. It is to be noted that the N and O elements in the PVP–AMPS polymer composite act as active centers. Further, they also perform as electrostatic forces between the inhibitor (PVP–AMPS) and the material of choice (copper and brass) [4]. In addition, the heterogeneous atoms (O and N) possess a strong ability to donate electrons, and thus the adsorption of the PVP–AMPS onto the surfaces of copper and brass results in an increase in the inhibition efficiency [35].

3.2.2 Effect of time

It is important to consider the effect of time when characterizing the corrosion inhibition efficiency of any corrosion inhibitor. The stability of the inhibitor film and the rate of adsorption of the inhibitor are estimated through immersion tests. The estimated IE of PVP–AMPS inhibitor against copper and brass coupons exposed for different time intervals and at different concentrations is given in Table 1 and is graphically represented in Figure 8. The maximum IE of PVP–AMPS inhibitor on copper and brass are 79.17% and 80.26%, respectively and these values are observed at the low immersion period of 3 h and a concentration of 800 ppm. It is observed that, at the longer immersion period of 24 h and a concentration of 50 ppm, the IE of PVP–AMPS on copper and brass is 18.37% and 19.62%, respectively, decreased significantly. On the other hand for all the concentrations of PVP–AMPS inhibitor tested on copper and brass coupons, a decrease in the IE is observed with the increase in the immersion time. Such a decrease in the IE can be due to the desorption process. During exposing the metal to corrosive media, the desorption of PVP–AMPS inhibitor from the surface of copper and brass takes place resulting in the decrease of IE and thereby increasing metal-solution contact [36], [37].

3.2.3 Effect of temperature

The temperature also has a major effect on the corrosion behavior of copper and brass in a corrosive environment specifically at the boiler room in desalination plants. The corrosion rates of copper and brass placed in different concentrations of PVP–AMPS measured at different temperatures are given in Table 2. It is observed that the increase in the temperature increases the corrosion rate. The increase in the corrosion rate can be attributed to the fact that when brass and copper are exposed to higher temperatures, they oxidize rapidly forming an unstable oxide layer. The formed oxide layer inhibits the reaction of the metal surface with the inhibitor by decreasing the reaction kinetics between the inhibitor and the metal surface. On the other hand, the variation of IE with the temperature of a corrosive environment is shown in Figure 9(a) and (b). It is observed that the maximum IE against copper and brass coupons is 72.22% and 80.26%, respectively, and is obtained at 298 K. As the temperature increases, the IE decreases and the lowest IE of 63.89% and 69.01% for copper and brass, respectively, is observed at the highest temperature of 333 K. Such a decrease in IE with temperature indicates the instability of PVP–AMPS inhibitor at higher temperatures. The instability may be due to the tendency of desorption. As a result of exothermic reactions at higher temperatures, desorption of the PVP–AMPS inhibitor from the surfaces of copper and brass takes place [38].

Table 1: Estimated IE of PVP–AMPS inhibitor against copper and brass coupons.

Concentration of PVP–AMPS (ppm)	Inhibitor Efficiency							
	Exposure Time (h) for Copper				Exposure Time (h) for Brass			
	3	9	12	24	3	9	12	24
Blank	0	0	0	0	0	0	0	0
50	20.83	19.73	18.37	17.56	24.52	22.62	20.61	19.62
100	27.78	25.44	22.09	20.7	32.68	25.17	23.03	21.74
200	37.5	34.94	30.65	28.02	40.82	31.73	27.52	25.42
300	44.44	37.45	35.47	31.51	53.37	40.9	38.96	32.9
400	52.78	43.08	41.78	35.58	57.99	46.49	42.57	40.67
500	55.56	47.42	44.19	41.63	63.91	52.15	47.66	45.94
600	65.28	58.5	52.19	48.95	67.74	62.18	58.06	53.75
700	73.61	67.41	64.31	59.53	79.58	69.63	66.96	61.96
800	79.17	69.83	67.54	64.42	80.26	74.49	70.77	66.79

Table 2: Effect of temperature on the corrosion rate of copper and brass in 1M HCl in the absence and presence of PVP–AMPS at various concentrations.

Temperature (K)	Corrosion Rate (mg $cm^{-2}h^{-1}$)					
	Concentrations PVP–AMPS for Copper (ppm)			Concentrations PVP–AMPS for Brass (ppm)		
	Blank	50	800	Blank	50	800
298	0	0.00124	0.0003	0	0.0125	0.0172
313	0	0.0221	0.0071	0	0.0189	0.0066
333	0	0.0136	0.0005	0	0.0657	0.0048

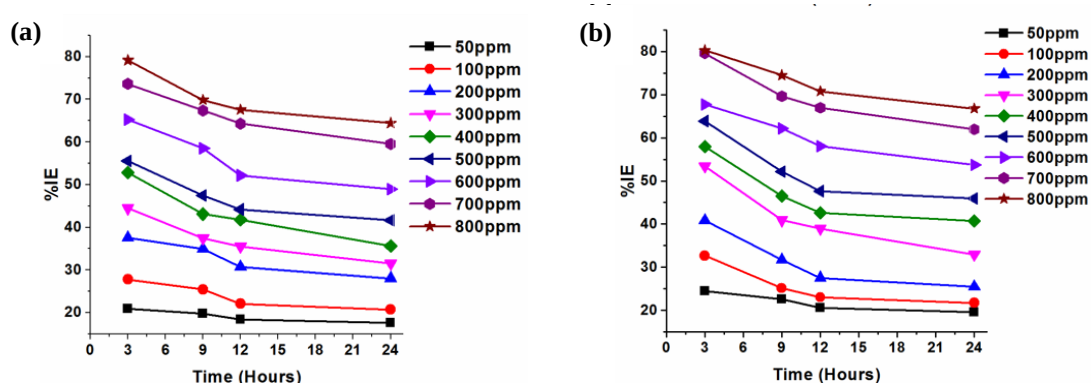

Figure 8: Variation of the inhibition efficiency of PVP–AMPS with varied exposure times of (a) copper and (b) brass.

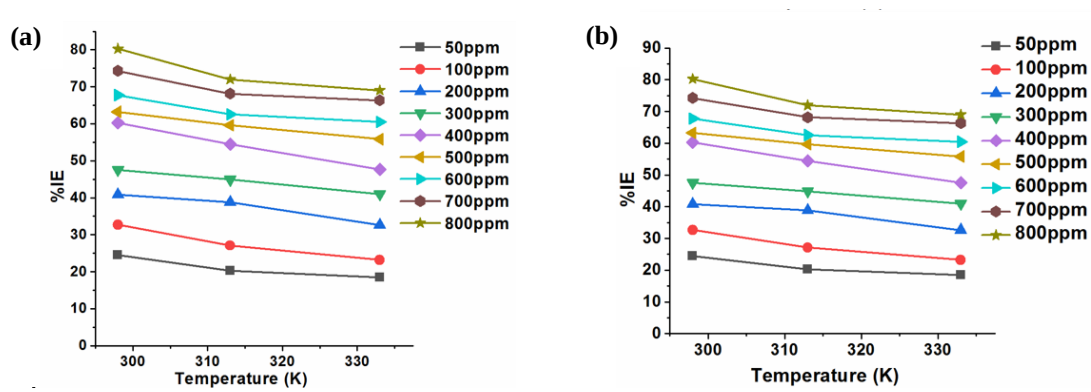

Figure 9: Variation of the inhibition efficiency of PVP–AMPS with varied exposure times of (a) copper and (b) brass.

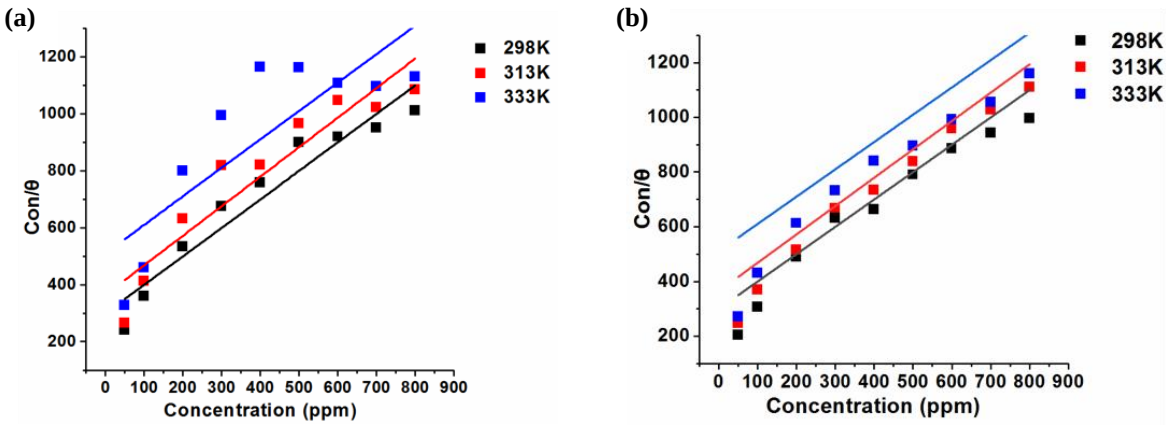

Figure 10: Langmuir adsorption isotherm plots obtained for (a) copper and (b) brass, immersed in varied concentrations of PVP–AMPS.

Table 3: Correlation coefficient (R^2) for PVP–AMPS on the surfaces of copper and brass.

Temperature (K)	Copper			Brass		
	Langmuir	Frumkin	Parsons-Temkin	Langmuir	Frumkin	Parsons-Temkin
298	0.9759	0.9877	0.9858	0.9428	0.9201	0.9251
313	0.9878	0.9303	0.7929	0.9925	0.9825	0.9801

3.2.4 Adsorption isotherm and adsorption parameters

Adsorption isotherms are essential to understand the interaction between the molecules of the PVP–AMPS inhibitor with the given metal substrates. Thus, the mechanism of inhibition can be understood [39]. In the current work, the isothermal principles, such as Langmuir, Frumkin, and Temkin-Parsons are studied. Using these isothermal principles, the variation in the surface coverage (θ) at varied concentrations of PVP–AMPS is estimated. The Langmuir adsorption isotherm is estimated using Equation (5).

$$\frac{C}{\theta} = \frac{1}{K_{ads}} + B \quad (5)$$

where θ is the surface coverage, C is the concentration of PVP–AMPS inhibitor, K is the equilibrium constant, and B is the intercept. A linear fit is established in the isothermal plots.

During the gravimetric analysis (weight loss tests), the surface coverage (θ) at different inhibitor concentrations on the surface of brass and copper respectively was evaluated. The mechanism of adsorption onto the surface of the substrate results in a higher degree and therefore greater inhibitive properties. Figure 10(a) and (b) show the Langmuir isotherm model plots for the dissolution of copper and brass respectively, which appeared to have close correlation coefficients. The dissolution of copper and brass showed a close relationship regarding the Langmuir plot. The estimated correlation coefficients (R^2), from the Langmuir, Frumkin, and Temkin-Parson's adsorption isotherms are tabulated in Table 3. It is observed from Table 3 that the Langmuir adsorption mechanism isotherm is the best fit with the best correlation close to unity. The data obtained from gravimetric analysis is further used to study the kinetic parameters of the system. The parameters like entropy, activation energy, and the enthalpy of adsorption of PVP–AMPS inhibitor on the surfaces of coupons are determined using the Arrhenius equation and the transition state equations. These parameters are determined for varied concentrations of PVP–AMPS inhibitor. The activation energy (E_a) of coupons is calculated using Equation (6).

$$\log CR = -\frac{E_a}{2.303RT} + \log A \quad (6)$$

Where (CR) is the corrosion rate, (E_a) is the activation energy, (R) is the molar gas constant, (T) is the absolute temperature, and (A) is the frequency factor. The log CR *vs* 1/T plots are shown in Figure 11. Both for copper and brass coupons, the plots show a linear relationship for different concentrations of PVP–AMPS inhibitor.

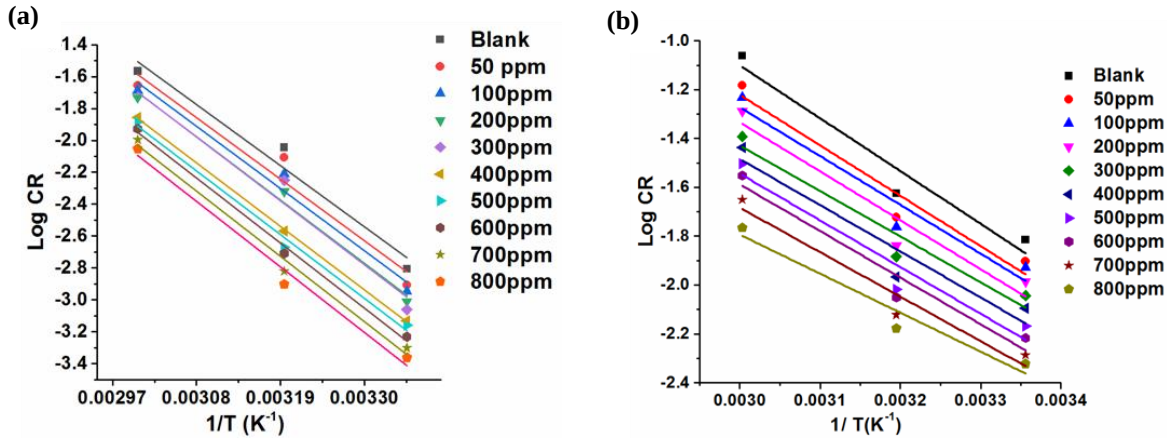

Figure 11: Arrhenius Plot for (a) copper and (b) brass in PVP–AMPS.

Table 4: Kinetic parameters of copper and brass dissolution in 1M HCl in the absence and presence of PVP–AMPS.

Concentration of PVP–AMPS (ppm)	Copper			Brass		
	E_a (kJmol^{-1})	ΔS (kJmol^{-1})	ΔH (kJmol^{-1})	E_a (kJmol^{-1})	ΔS (kJmol^{-1})	ΔH (kJmol^{-1})
Blank	28.6	−251.04	13.72	17.97	−200	13.46
50	28.8	−254.48	13.72	17.17	−194.79	13.44
800	32.2	−289.53	13.78	21.29	−165.15	13.35

Table 5: Free energy absorption (ΔG_{ads} (kJmol^{-1}) of copper and brass at different temperatures.

Concentration of PVP–AMPS (ppm)	Copper			Brass		
	298 K	313 K	333 K	298 K	313 K	333 K
Blank	0	0	0	0	0	0
50	−10.65	−11.18	−11.89	−11.39	−11.97	−12.73
800	−9.98	−10.49	−11.16	−9.24	−9.71	−10.33

The activation energy ($-\frac{E_a}{2.303R}$) is estimated by the slope of the curves in the plots. The estimated values are given in Table 4. In the case of copper samples, the activation energy of the blank solution is 28.62 KJmol^{-1} and for the concentration of 800 ppm, the activation energy increases to 32.22 KJmol^{-1}. Similarly for brass, it increases from 17.97 KJmol^{-1} to 21.29 KJmol^{-1}. Such an increase in activation energy confirms the adsorption of the PVP–AMPS inhibitor onto the surfaces of both copper and brass. The adsorption is due to the decrease in the surface area available for metal dissolution. The heteroatoms in the PVP–AMPS inhibitor result in an increased rate of reaction [4], [40].

To study the inhibitive mechanism, strength, and mode of adsorption of the PVP–AMPS inhibitor, the thermodynamic parameters are estimated. At different concentrations and temperatures, the resultant surface coverages ΔG_{ad} is calculated using Equation (7).

$$\Delta G = -RT\ln(55.5K_{ads}) \quad (7)$$

Where (T) is the temperature, R=8.314 is the molar gas constant, 55.5 is the molar concentration of water, and (K_{ads}) is the equilibrium constant of adsorption. The (K_{ads}) is determined from the intercept of the Langmuir adsorption isotherm plot. The calculated ΔG values at various temperatures are given in Table 5. The ΔG values are negative which indicates the spontaneity of adsorption of the adsorbed layer on copper and brass surfaces. The adsorption mechanism is the physisorption process if the $|\Delta G_{ads}|$ is less than 20 kJmol^{-1} and is the chemisorption process if the $|\Delta G_{ads}|$ is less than 40 kJmol^{-1} [4]. From Table 5, it is clear that in the current study, the physisorption process was dominant. Further, with an increase in temperature, IE decreases due to the electrostatic interaction between the PVP–AMPS inhibitor and the surfaces of copper and brass shows. Using the Gibbs Helmholtz relation given in Equation (8), the enthalpy (ΔH) and the entropy (ΔS) of adsorption are calculated.

Further, the values of enthalpy (ΔH_a) and entropy (ΔS_a) for the activation of the dissolution of copper and brass are calculated using Equation (9).

$$\frac{\log CR}{T} = \log\left(\frac{R}{nh}\right) + \frac{\Delta S_a}{2.303R} - \frac{\Delta H_a}{2.303T} \quad (9)$$

Where (n) was Avogadro's constant and (h) is the Planck's constant. The plots of log (CR/T) *vs* 1/T at different concentrations of PVP–AMPS with copper and brass are shown in Figure 12(a) and (b). The plots depict a linear relationship.

3.3 *Electrochemical and surface analytical studies*

The Tafel experimental data is tabulated in Table 6 and is used to estimate the instantaneous corrosion rate of copper and brass at different concentrations of PVP–AMPS. The polarization plots for the copper and brass at different concentrations of the PVP–AMPS inhibitor are given in Figure 13(a) and (b).

The Tafel plots for both copper and brass exhibit cathodic and anodic reaction that results in the cathodic current. The cathodic reaction indicates the decreasing evolution of hydrogen and the anodic reaction indicates an active-passive transition [41]. Further, the formation of two anodic peaks followed by a permanent passive region indicates active dissolution [42]. The drop in the anodic current is due to the adsorption process. As the reaction proceeds, the oxidation of copper and brass continues to form oxide films on the surfaces as a result of the adsorption of $CuCl_{ads}$ and $ZnCl_{ads}$ species. Such films hinder the further dissolution process resulting in the drop [30]. It can also be noted that there exists a shift in anodic and cathodic branches in the presence of the PVP–AMPS inhibitor and the shift is towards smaller current densities. Such a shift of branches indicates that the PVP–AMPS composite behaves as a mixed-type inhibitor [40], [43]. Tafel slopes (β_c and β_a) are calculated by the extrapolation of the Tafel polarization plot. The extrapolated values are given in Table 6. It is observed that in the presence of the PVP–AMPS inhibitor, the cathodic and anodic Tafel slopes are changing [43].

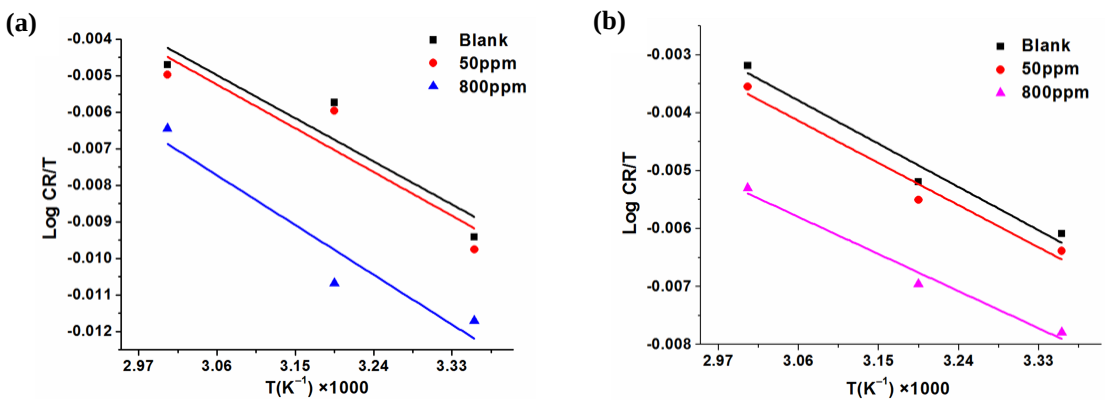

Figure 12: Transition state plot of (a) Copper and (b) Brass at different concentrations of PVP–AMPS.

Table 6: Tafel parameters of the dissolution of copper and brass in different concentrations of PVP–AMPS.

Concentration of PVP–AMPS (ppm)	Copper				Brass			
	E_{corr}	I_{corr}	βa	βc	E_{corr}	I_{corr}	βa	βc
Blank	−345.41	278.94	90.8	155.2	−360.17	291.41	78.1	107.6
200	−343.82	169.87	77.7	138.10	−356.66	172.28	83.1	208.3
300	−356.31	144.46	86.5	126.14	−357.47	130.87	82.6	111.5
400	−352.29	128.16	87.2	124.59	−362.12	108.77	84.9	108.2
500	−360.26	118.86	87.3	108.11	−360.33	93.10	88.6	124.6
600	−365.22	94.30	83.8	205.79	−344.15	74.33	82.3	152.1
700	−361.09	62.56	88.9	114.32	−346.67	63.21	76.0	119.8
800	−339.77	55.23	65.4	145.45	−333.39	54.527	65.9	125.2

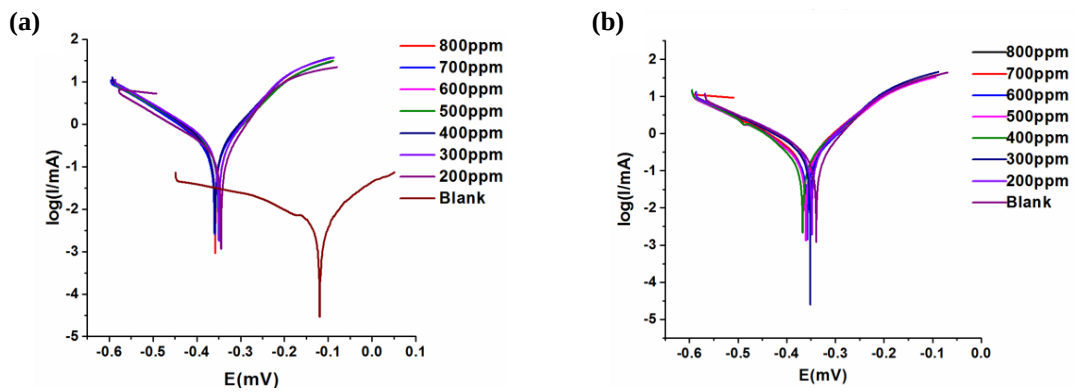

Figure 13: Tafel plot for (a) Copper and (b) Brass in a blank HCl solution and various concentrations of PVP–AMPS.

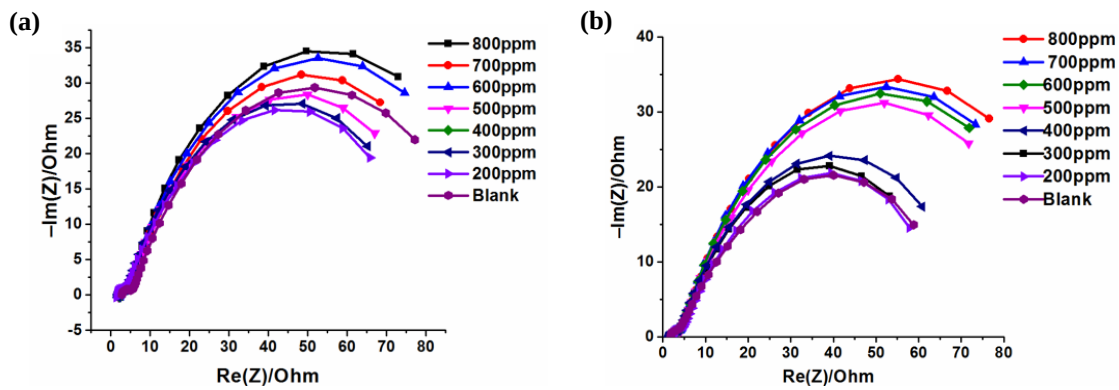

Figure 14: Nyquist plot for (a) Copper and (b) Brass at various concentrations of PVP–AMPS.

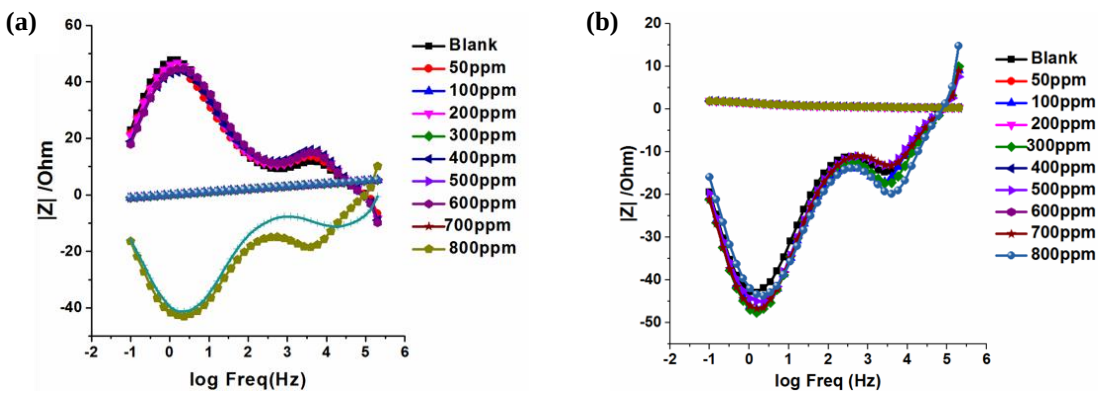

Figure 15: Bode plots for (a) Copper and (b) Brass at various concentrations of PVP AMPS.

While the cathodic Tafel slope β_c changes with the concentration of PVP–AMPS inhibitor, the anodic β_a slope indicates that the change is due to the adsorption of the inhibitor PVP–AMPS onto the surfaces of copper and brass. As a result of adsorption phenomena, the PVP–AMPS inhibitor film is formed film on the surfaces of copper and brass. The adsorption includes interactions between the π-electrons of the heterocyclic structure of PVP–AMPS inhibitor and the vacant d-orbitals of copper and brass surface atoms. Further, the type of the inhibitor i.e., an anodic and a cathodic inhibitor, is decided based on the shift in E_{corr}. In the case of the E_{corr}>85 mV as compared to the blank solution, it indicates that both reactions are affected by the inhibitor [4], [44], [45].

Table 7: Potentiodynamic polarization IE data for Copper and Brass in 1M HCl.

Concentration of PVP–AMPS (ppm)	Copper		Brass	
	I_{corr}	%IE	I_{corr}	%IE
Blank	278.94	0	291.41	0
200	169.87	39.10	172.28	40.88
300	144.46	48.21	130.87	55.09
400	128.16	54.05	108.77	62.70
500	118.86	57.38	93.10	68.05
600	94.30	66.19	74.33	74.49
700	62.56	77.57	63.21	78.30
800	55.23	80	54.527	81

The corrosion densities for copper and brass at different concentrations of PVP–AMPS are given in Table 7. The corrosion current density (observed in the case of the blank solution) is despaired by the addition of the inhibitor at different concentrations [46]. It is observed from Table 7 that the current corrosion density (I_{corr}) decreases with the increase in the concentration of PVP–AMPS. The inhibition efficiency was calculated using Equation 10. The calculated IE values are included in the Table 7. It is observed in Table 7 that the corrosion current densities are smaller than the blank solution. Also, the IE increases with an increase in the concentration of PVP–AMPS, and at 800 ppm, the IE is 80% and 81% for copper and brass respectively.

$$IE = \frac{I_{corr(blank\ HCl)} - I_{corr(PVP-AMPS)}}{I_{corr(PVP-AMPS)}} \times 100 \quad (10)$$

3.3.1 Electrochemical Impedance Spectroscopy of PVP–AMPS

The Nyquist plots for copper and brass at various concentrations of PVP–AMPS are shown respectively in Figure 14(a) and (b). The Bode plots for copper and brass are shown in Figure 15(a) and (b).

It is observed from the Nyquist plots that an increase in the concentration of the PVP–AMPS corrosion inhibitor enhances the corrosion inhibition efficiency. The spectra in both copper and brass are characterized by two slightly distorted semicircles one at a higher and the other at a lower frequency [47].

Table 8: EIS parameters for Copper and Brass at different concentrations of PVP–AMPS.

Concentration of PVP–AMPS (ppm)	Copper							Brass						
	R_1 (Ohm)	Q_1 $\times 10^{-3}$	a_1	R_2 (Ohm)	Q_3 $\times 10^{-3}$	a_3	R_3 (Ohm)	R_1 (Ohm)	$Q_1 \times 10^{-3}$	a_1	R_2 (Ohm)	Q_3 $\times 10^{-3}$	a_3	R_3 (Ohm)
Blank	1.72	0.37	0.91	2.88	9.64	0.52	55.73	2.26	0.16	0.64	1.57	8.71	0.18	0.08
200	2.72	0.32	0.77	2.37	9.75	0.71	102.00	1.87	8.46	0.47	4.58	1.84	1.00	146.10
300	4.46	0.17	0.82	2.32	8.69	0.72	105.73	1.88	0.16	0.84	4.98	8.56	0.73	103.18
400	4.99	4.90	0.49	4.63	5.07	0.81	98.69	2.39	0.19	0.84	5.33	8.59	0.71	98.47
500	5.42	5.35	0..52	3.96	4.94	0.83	96.28	2.07	9.86	0.46	5.80	1.91	1.00	103.81
600	5.75	5.25	0.50	3.75	4.83	0.81	95.00	1.09	0.09	0.88	6.25	9.11	0.69	78.91
700	6.31	9.96	0.44	7.94	1.48	0.99	87.75	2.14	0.17	0.84	6.86	9.06	0.68	72.26
800	6.92	0.2	0.67	2.82	6.56	0.70	96.33	1.81	0.13	0.86	1.57	9.28	0.63	78.14

As discussed earlier, as a result of desorption there is a formation of a copper-oxide and zinc-oxide film on the surfaces of copper and brass respectively. The oxide layer on the surface of the samples reflects as a semicircle at a higher frequency. Similarly, the diffusion of $CuCl_2$ and the $ZnCl_2$ charge into the solution reflects as the second semicircle in the bode plots, and the diffusion is determined by the Warburg parameter [5], [47]–[50]. The results also suggest that the PVP–AMPS composite obeyed the Langmuir adsorption isotherm for adsorption on the surfaces of copper and brass. In the low-frequency region observed in the Bode plot, the |Z| increases with a decrease in frequency due to the diffusion of oxygen and chloride from the solution resulting in longer immersion times. As the concentration of the inhibitor increases, the |Z| value increases, and thus the resistance against corrosion increases. At optimal inhibitor concentrations, defect-less layers with promising inhibition are seen in the Bode plots. The equivalent electrical circuit (ECC) in Figure 16 is used to show the behavior of copper and brass respectively in the presence of PVP–AMPS. The EIS parameters for both copper and brass are given in Table 8.

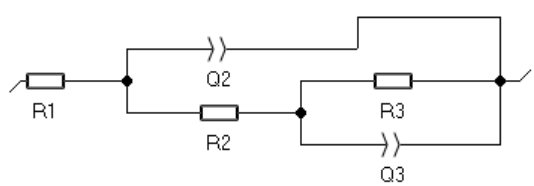

Figure 16: An equivalent circuit model was used to analyze the electrical behavior.

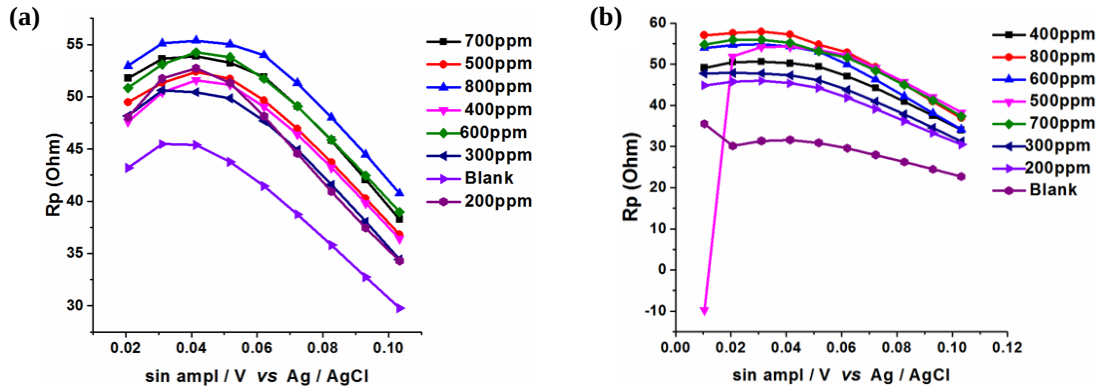

Figure 17: VASP plots for (a) Copper and (b) Brass at different concentrations of PVP–AMPS.

In the circuit (Figure 16), the R_1 element indicates the solution resistance, the R_2 element indicates the charge resistance (R_{ct}) of both copper and brass and the R_3 element represents the resistance to charge transfer as a result of the formation of inhibitor film. The Q_2 and Q_3 are constant phase elements that represent the layer between the metal solution interface before and after the formation of the thin-film layer. The calculated EIS parameters are given in Table 8. The corresponding IE based on the EIS parameters are given in Table 9.

Table 9: Corrosion efficiencies for copper and brass calculated from EIS.

Concentration of PVP–AMPS (ppm)	Copper		Brass	
	Rct (Ohm/cm^2) × 10^2	IE	Rct (Ohm/cm^2) × 10^2	IE
Blank	1.70	0	1.57	0
200	2.72	37.5	2.65	40.8
300	4.46	61.9	4.58	65.7
400	4.99	65.9	4.98	68.5
500	5.42	68.6	5.33	70.5
600	5.75	70.4	5.80	72.9
700	6.31	73.1	6.25	74.9
800	6.92	75.4	6.86	77.1

Table 10: VASP Parameters of copper and brass at different concentrations of PVP–AMPS.

Concentration of PVP–AMPS (ppm)	Copper		Brass	
	R_p (×10) Ohm	% IE	R_p (×10) Ohm	% IE
Blank	4.25	0	3.5	0
200	4.75	10.5	4.5	22.2
300	4.76	10.7	4.6	23.9
400	4.8	11.5	4.9	28.6
500	4.9	13.3	5.1	31.4
600	5.15	17.5	5.3	34
700	5.2	18.3	5.5	36.4
800	5.35	20.6	5.7	38.6

It is observed that, in the presence of the PVP–AMPS inhibitor, the values of R_{ct} and the resultant inhibition efficiency increase. The increase is attributed to the formation of a protective film at the interfaces between the metal (copper and brass) and HCl [41]. The charge transfer resistance (R_2) and the layer of resistance (R_1) for the copper and brass at the various concentrations of PVP–AMPS, increases as compared to the blank solution and the increase is due to the hindering of the oxygen diffusion onto the surfaces of the copper and brass. The resistance in the blank solution for copper and brass is 1.703×10^2 Ohm/cm^2 and 1.57×10^2 Ohm/cm^2 respectively while in the presence of PVP–AMPS, the charge transfer resistance increases. At the concentration of 800 ppm, the charge transfer resistance for copper and brass is 6.917×10^2 Ohm/cm^2 and 6.862×10^2 Ohm/cm^2, respectively. However, the capacitance decreases and is attributed to the adsorption mechanism of PVP–AMPS, and also the increase in the charge transfer resistance results in a decrease in the metal oxidation reaction [43], [51].

3.3.2 Variable Amplitude Micro-Sinusoidal Polarization (VAMSP) Studies of PVP–AMPS

The polarization resistance (R_p) was determined using VASP. The calculated resistance and the corresponding IE values are listed in Table 10. Figure 17(a) and (b) show the plots of R_p *vs* sine amplitude for the dissolution of copper and brass at different concentrations of PVP–AMPS.

Depending on the dominance of the reaction, polarization may take place either on the anodic or cathodic side, and in the present case, the cathodic side was more dominant, and hence both copper and brass were cathodically polarized [52]. The VASP

inhibition efficiency of copper and brass at different concentrations of PVP–AMPS is calculated using Equation (11).

$$IE = \frac{R_p - R_p^0}{R_p} \times 100 \quad (11)$$

where R_p is the polarization resistance of the electrode with the presence of PVP–AMPS inhibitor and $R^0{}_p$ is the polarization resistance of copper and brass in the blank solution. The R_p of the system increases with increasing concentrations of the PVP–AMPS inhibitor. The increase in R_p is also due to the film formation of the inhibitor (PVP–AMPS) on the surfaces of copper and brass as the concentration is increased. Increasing the concentration of the PVP–AMPS offers more active sites for the absorption process to take place consequently protection is increased by the formation of the protective film.

4 Discussion

The process parameters for corrosion inhibition for current work were concentration, exposure time, and temperature. The effect of each parameter was studied; however, it was also important to understand the phenomena (thermodynamic, kinetics, and electrochemical) that exactly enhance the inhibition performance of the PVP–AMPS composite. The current studies first distinguished the microstructural features of AMPS, PVP copolymer, and PVP–AMPS composite. These characteristics were studied using SEM, XRD, and FTIR techniques. A distinguished difference in microstructure was observed. The AMPS exhibited various interconnected uniformly sized pores. It is suggested that these pores were the result of significant mobility related to a flexible microstructure and water-binding ability of AMPS [53]. A similar observation was also reported by Shaban *et al*. [54] On the other hand, the PVP copolymer envisages a spherical-shaped microstructure; a similar spherical-shaped microstructure was reported in earlier findings [55], [56]. It is suggested that the spherical agglomeration and spherical crystallization envisage this specific microstructure [57]. The PVP–AMPS composite microstructure envisages a rod-like morphology due to the directional growth of crystals envisaged by interfaces [58].

The gravimetric studies considering weight loss tests envisage a decreasing corrosion rate (or increasing corrosion inhibition) with a concentration of PVP–AMPS. It is suggested that the higher concentration leads to the higher solubility of PVP–AMPS in the corrosive medium. Karthikaiselvi *et al*., studied similar studies for mild steel in HCL solution; they reported that the PVP–AMPS inhibited corrosion at all (100–2000 ppm) concentrations [34]. The corrosion inhibition was related to electronegative atoms like oxygen (O) and nitrogen (N) in the crystal; the PVP–AMPS contained heterogeneous atoms (O and N) having the ability to transfer the electron, which further leads to the envisaged adsorption phenomena [35]. The desorption process plays an important role in IR% for copper and brass; a higher exposure time in the corrosive media increases the desorption, which leads to a decrease in IR%. This process envisages an adsorbed atom/molecule to be released in the corrosive medium (HCL). It is suggested that the molecules gained the chemical energy supplied by the corrosive medium to overcome the activation barrier and the binding energy [59], [60].

Corrosion is proportional to the rate of diffusion, which increases at higher temperatures vis-à-vis the electrolytic resistance decreases [61], [62]. The exothermic reactions are also favorable at higher temperatures, which accelerates desorption of the PVP–AMPS inhibitor, and hence the corrosion inhibition decreases with temperature. It is also important to understand that if the temperature is raised beyond a critical limit the rate of corrosion decreases, however in current studies this temperature range was not achieved in present experimental conditions [63]. The current studies further considered adsorption Isotherm process parameters which exhibited the best correlation coefficient (R^2) for the Langmuir adsorption mechanism for given experimental conditions. However, it is suggested that with a change in process parameters other adsorption mechanisms like Frumkin, and Temkin-Parsons may be dominant [64], [65]. It was felt that the hypothesis of the adsorption process needs to be validated; hence other thermodynamics process parameters considering entropy, activation energy, and the enthalpy of adsorption were studied using Arrhenius and transition state equation. The hypothesis of the adsorption process was validated considering the increasing activation energy. The resultant surface coverages ΔG_{ad} were calculated for different temperatures and concentrations to study the inhibitive mechanism, strength, and mode of adsorption. The $|\Delta G_{ads}|$ was less than 20 $kJmol^{-1}$ envisaging the process was a physisorption rather than chemisorption.

On the other hand, the electrochemical and surface analytical studies also confirm the adsorption

process; a drop in the anodic current suggests the phenomena. The adsorption of $CuCl_{ads}$ and $ZnCl_{ads}$ envisages the formation of oxide films on the surfaces; these films hinder the corrosion process. There was a shift in anodic and cathodic branches in the presence of the PVP–AMPS inhibitor indicating a mixed-type inhibitor behavior of the PVP–AMPS composite. A change in cathodic and anodic Tafel slopes (β_c and β_a) with the concentration of PVP–AMPS inhibitor also supports the adsorption phenomena. The similar observation from Nyquist plots once again validated the dependence of corrosion inhibition on concentration. Variable amplitude micro-sinusoidal polarization studies were done considering the polarization resistance of the electrode with the presence of PVP–AMPS inhibitor and the same in the blank solution for comparison. The increasing concentration envisages a similar effect on corrosion inhibition as confirmed by other adopted characterization techniques in the current studies.

5 Conclusions

The following are the major conclusions drawn from the present work. The polymerization between PVP and AMPS was achieved; the disappearance of the peaks at 3000–3100 cm^{-1} in FTIR spectra was due to the stretching vibration of HC during the crosslinking polymerization. The O-H peak was not observed in the PVP–AMPS composite indicating the removal of water molecules during the polymerization process. The PVP copolymer exhibited the spherical-shaped microstructure; when it polymerized with the AMPS having several interconnected uniformly sized pores, it produced a PVP–AMPS composite with rod-like microstructure.

The effect of concentration, time, and temperature on the corrosion inhibition efficiency of the PVP–AMPS composite was studied. The IE increases with concentration and decreases with time and temperature. The increase in IE with concentration was attributed to the solubility of PVP–AMPS composite in HCl; however, the decrease in IR with time and temperature was due to the "desorption of PVP–AMPS composite from the surface of copper and brass" and exothermic reactions at higher temperature, respectively.

The adsorption isotherm process envisages the best correlation coefficient (R^2) for the Langmuir adsorption mechanism. The hypothesis of the adsorption process was also validated considering the increasing activation energy. The ΔG values were negative indicating the spontaneity of the adsorption process and the $|\Delta G_{ads}|$ was less than 20 $kJmol^{-1}$ envisaging the process was a physisorption rather than chemisorption.

The adsorption of $CuCl_{ads}$ and $ZnCl_{ads}$ was due to the formation of oxide films, these films hinder the corrosion process. There was a shift in anodic and cathodic branches in the presence of the PVP–AMPS inhibitor indicating a mixed-type inhibitor behaviour of the composite. A change in cathodic and anodic Tafel slopes (β_c and β_a) with the concentration of PVP–AMPS inhibitors was observed.

Based on the current studies, the PVP–AMPS composite (also an eco-friendly material) showed excellent corrosion inhibition efficiency in an acidic medium. Therefore, it can be used in copper and its alloys which are susceptible to corrosion in heat exchangers and coolers specifically during acid cleaning, and impede and prohibit the materials loss due to the corrosion process.

Acknowledgments

The authors wish to acknowledge the Department of Metallurgy-University of Johannesburg, South Africa, and The State Scientific Institution-The Joint Institute of Mechanical Engineering of The National Academy of Sciences of Belarus.

Author Contributions

M.E.M.: conceptualization, methodology, project administration; M.G.T.: experiments, investigation; L.M.Y.: experiments, investigation, writing an original draft; S.S.: conceptualization, methodology; D.P.: conceptualization, methodology; V.H.M.: research design, writing—reviewing and editing; P.K.: data analysis, writing—reviewing and editing. All authors have read and agreed to the published version of the manuscript.

Conflicts of Interest

The authors declare no conflict of interest.

References

[1] L. Feng, C. Yin, H. Zhang, Y. Li, X. Song, Q. Chen, and H. Liu, "Cationic gemini surfactants with a bipyridyl spacer as corrosion inhibitors for carbon steel," *ACS Omega*, vol. 3, no. 12, pp. 18990–18999, Dec. 2018, doi: 10.1021/acsomega.

8b03043.
[2] P. M. Niamien, H. A. Kouassi, A. Trokourey, F. K. Essy, D. Sissouma, and Y. Bokra, "Copper corrosion inhibition in 1 M HNO_3 by two benzimidazole derivatives," *International Scholarly Research Notices*, vol. 2012, pp. 1–15, 2012, doi: 10.5402/2012/623754.
[3] T. L. Skovhus, R. B. Eckert, and E. Rodrigues, "Management and control of microbiologically influenced corrosion (MIC) in the oil and gas industry—Overview and a North Sea case study," *Journal of Biotechnology*, vol. 256, pp. 31–45, 2017, doi: 10.1016/j.jbiotec.2017.07.003.
[4] M. G. Tsoeunyane, M. E. Makhatha, and O. A. Arotiba, "Corrosion inhibition of mild steel by poly(butylene succinate)-L-histidine extended with 1,6-diisocynatohexane polymer composite in 1 M HCl," *International Journal of Corrosion*, vol. 2019, 2019, doi: 10.1155/2019/7406409.
[5] N. Mahato and M. M. Singh, "Investigation of passive film properties and pitting resistance of AISI 316 in aqueous ethanoic acid containing chloride ions using electrochemical impedance spectroscopy(EIS)," *Portugaliae Electrochimica Acta*, vol. 29, pp. 233–251, 2011, doi: 10.4152/pea.201104233.
[6] S. Ramesh, G. Anne, N. Bhat, G. Aithal, H. Shivananda Nayaka, and S. Arya, "Surface modification of multi-directional forged biodegradable Mg-Zn alloy by ball burnishing process: Modeling and analysis using deep neural network," *Journal of Manufacturing Processes*, vol. 68, pp. 423–434, 2021, doi: 10.1016/j.jmapro.2021.05.049.
[7] G. Anne, M. R. Ramesh, H. Shivananda Nayaka, S. B. Arya, and S. Sahu, "Microstructure evolution and mechanical and corrosion behavior of accumulative roll bonded Mg-2%Zn/Al-7075 multilayered composite," *Journal of Materials Engineering and Performance*, vol. 26, no. 4, pp. 1726–1734, 2017, doi: 10.1007/s11665-017-2576-z.
[8] N. U. Shehu, U. I. Gaya, and A. A. Muhammad, "Influence of side chain on the inhibition of aluminium corrosion in HCl by α-amino acids," *Applied Science and Engineering Progress*, vol. 12, no. 3, pp. 186–197, Aug. 2019, doi: 10.14416/j.asep.2019.07.002.
[9] O. Falodun and R. Loto, "Corrosion behavior of AA70 reinforced zea mays husk particle in NaCl/H_2SO_4 concentrations," *Applied Science and Engineering Progress*, vol. 17, no. 1, Feb. 2024, Art. no. 6915, doi: 10.14416/j.asep.2023.08.001.
[10] M. Oki, A. A. Adediran, A. Ikechukwu, C. O. Onokohwomo, C. Bosa, S. A. Akintola, and O. S. Adesina, "Corrosion protection by novel conversion coatings on structural Al 6061," *Applied Science and Engineering Progress*, vol. 16, no. 1, Nov. 2022, Art. no. 5806, doi: 10.14416/j.asep.2022.03.005.
[11] S. Daopiset, N. Karnchanaprayut, N. Kiatsareekul, and T. Kongkrapan, "Effects of surface finishes on corrosion resistance of welded stainless steels," *Applied Science and Engineering Progress*, vol. 3, no. 3, pp. 65–71, Sep. 2013.
[12] A. S. Fouda, M. A. Ismael, R. M. Abo Shahba, L. A. Kamel, and A. A. El-Nagggar, "Corrosion inhibition of copper and α-brass in 1 M HNO3 solution using new arylpyrimido [5, 4-c] quinoline-2,4-dione derivative," *International Journal of Electrochemical Science*, vol. 12, no. 4, pp. 3361–3384, 2017, doi: 10.20964/2017.04.57.
[13] L. Chen, D. Lu, and Y. Zhang, "Organic compounds as corrosion inhibitors for carbon steel in hcl solution: A comprehensive review," *Materials*, vol. 15, no. 6, 2022, doi: 10.3390/ma15062023.
[14] W. Guo, C. Gao, Q. Li, Z. Cheng, and X. Qi, "Preparation of scale inhibitor by using the waste of refined 2-acrylamido-2-methylpropane sulfonic acid," *Environmental Progress & Sustainable Energy*, vol. 35, no. 3, pp. 833–839, May 2016, doi: 10.1002/ep.12290.
[15] A. Singh, M. Liu, E. Ituen, and Y. Lin, "Anti-corrosive properties of an effective guar gum grafted 2-Acrylamido-2-Methylpropanesulfonic acid (GG-AMPS) coating on copper in a 3.5% NaCl solution," *Coatings*, vol. 10, no. 3, 2020, doi: 10.3390/coatings10030241.
[16] L. A. Al Juhaiman, "Polyvinyl pyrrolidone as a corrosion inhibitor for carbon steel in HCl," *International Journal of Electrochemical Science*, vol. 11, no. 3, pp. 2247–2262, 2016, doi: 10.1016/s1452-3981(23)16098-6.
[17] Y. Chen and W. Yang, "Formulation of corrosion inhibitors," in *Water Chemistry*, M. Eyvaz and E. Yüksel, Eds. Rijeka: IntechOpen, 2020, doi: 10.5772/intechopen.88533.
[18] C. Zhichun, L. Jianzhong, Z. Zhiying, Y. Wenhu, and Q. Donghai, "Effects of addition of polyvinyl pyrrolidone (PVP) as a corrosion

inhibitor to Zr/V-based conversion coating on aluminum alloy," *Chemical Papers*, vol. 77, no. 10, pp. 5847–5857, 2023, doi: 10.1007/s11696-023-02902-4.

[19] S. A. Umoren and E. E. Ebenso, "Blends of polyvinyl pyrrolidone and polyacrylamide as corrosion inhibitors for aluminium in acidic medium," *Indian Journal of Chemical Technology*, vol. 15, no. 4, pp. 355–363, 2008.

[20] R. Salim, E. Ech-chihbi, H. Oudda, F. El Hajjaji, M. Taleb, and S. Jodeh, "A review on the assessment of imidazo[1,2-a]pyridines as corrosion inhibitor of metals," *Journal of Bio- and Tribo-Corrosion*, vol. 5, no. 1, pp. 1–9, 2019, doi: 10.1007/s40735-018-0207-3.

[21] X. Wang, S. Liu, J. Yan, J. Zhang, Q. Zhang, and Y. Yan, "Recent progress of polymeric corrosion inhibitor: Structure and application," *Materials*, vol. 16, no. 8, Apr. 2023, doi: 10.3390/ma16082954.

[22] S. A. Umoren, "Polymers as corrosion inhibitors for metals in different media- A review," *The Open Corrosion Journal*, vol. 2, no. 1, pp. 175–188, 2009, doi: 10.2174/1876503300902010175.

[23] A. F. Sabirneeza and S. Subhashini, "Synergistic influence of leucine on polyvinyl alcohol in the corrosion inhibition of mild steel in molar hydrochloric acid – taguchi method," *Research Journal of Chemical Sciences*, vol. 43, no. 3, pp. 10–16, 2014, doi: 10.15764/ojces.2014.01007.

[24] A. Ali Fathima Sabirneeza and S. Subhashini, "A novel water-soluble, conducting polymer composite for mild steel acid corrosion inhibition," *Journal of Applied Polymer Science*, vol. 127, no. 4, pp. 3084–3092, Feb. 2013, doi: 10.1002/app.37661.

[25] D. V. Ribeiro and J. C. C. Abrantes, "Application of electrochemical impedance spectroscopy (EIS) to monitor the corrosion of reinforced concrete: A new approach," *Construction and Building Materials*, vol. 111, pp. 98–104, 2016, doi: 10.1590/s1983-41952015000400007.

[26] H. Jamshidi and A. Rabiee, "Synthesis and characterization of acrylamide-based anionic copolymer and investigation of solution properties," *Advances in Materials Science and Engineering*, vol. 2014, p. 728675, 2014, doi: 10.1155/2014/728675.

[27] R. P. Amelia, S. Gentile, W. F. Nirode, and L. Huang, "Quantitative analysis of copolymers and blends of polyvinyl acetate (PVAc) using fourier transform infrared spectroscopy (FTIR) and elemental analysis (EA)," *World Journal of Chemical Education*, vol. 4, no. 2, pp. 25–31, May 2016, doi: 10.12691/wjce-4-2-1.

[28] A. Awadallah-F, S. Y. A. El-Wahab, and H. I. Al-Shafey, "Controlled synthesis and characterization of nanohydrogels formed from copolymer (2-acrylamido-2-methylpropane sulfonic acid/acrylamide)," *e-Polymers*, vol. 16, no. 3, pp. 207–215, 2016, doi: 10.1515/epoly-2015-0263.

[29] A. M. Atta, R. A. M. El-Ghazawy, R. K. Farag, and S. M. Elsaeed, "Synthesis and characterization of pH-sensitive PAMPS/PVP nanogels in aqueous media," *Polymers for Advanced Technologies*, vol. 22, no. 5, pp. 732–737, May 2011, doi: 10.1002/pat.1573.

[30] J. Breton, "Fourier transform infrared spectroscopy of primary electron donors in type I photosynthetic reaction centers," *Biochimica et Biophysica Acta (BBA) - Bioenergetics*, vol. 1507, no. 1, pp. 180–193, 2001, doi: 10.1016/S0005-2728(01)00206-7.

[31] K. Chhouk, Wahyudiono, H. Kanda, S.-I. Kawasaki, and M. Goto, "Micronization of curcumin with biodegradable polymer by supercritical anti-solvent using micro swirl mixer," *Frontiers of Chemical Science and Engineering*, vol. 12, no. 1, pp. 184–193, 2018, doi: 10.1007/s11705-017-1678-3.

[32] D. Pathania and R. Sharma, "Synthesis and characterization of graft copolymers of methacrylic acid onto gelatinized potato starch using chromic acid initiator in presence of air," *Advanced Materials Letters*, vol. 3, no. 2, pp. 136–142, 2012, doi: 10.5185/amlett.2011.8297.

[33] R. K. Mishra, M. Datt, and A. K. Banthia, "Synthesis and characterization of pectin/PVP hydrogel membranes for drug delivery system," *AAPS PharmSciTech*, vol. 9, no. 2, pp. 395–403, 2008, doi: 10.1208/s12249-008-9048-6.

[34] R. Karthikaiselvi and S. Subhashini, "The water soluble composite poly(vinylpyrrolidone–methylaniline): A new class of corrosion inhibitors of mild steel in hydrochloric acid media," *Arabian Journal of Chemistry*, vol. 10, no. 1, pp. S627–S635, 2017, doi: 10.1016/j.arabjc.2012.10.024.

[35] S. Xu, S. Zhang, L. Guo, L. Feng, and B. Tan, "Experimental and theoretical studies on the corrosion inhibition of carbon steel by two indazole derivatives in HCl medium," *Materials*, vol. 12, no. 8, Art. no. 1339, Apr. 2019, doi: 10.3390/ma12081339.

[36] M. H. Sliem, M. Afifi, A. Bahgat Radwan, E. M. Fayyad, M. F. Shibl, F. E.-T. Heakal, and A. M. Abdullah, "AEO7 surfactant as an eco-friendly corrosion inhibitor for carbon steel in HCl solution," *Scientific Reports*, vol. 9, no. 1, Art. no. 2319, Feb. 2019, doi: 10.1038/s41598-018-37254-7.

[37] P. Arockiasamy, X. Q. R. Sheela, G. Thenmozhi, M. Franco, J. W. Sahayaraj, and R. J. Santhi, "Evaluation of corrosion inhibition of mild steel in 1 M hydrochloric acid solution by mollugo cerviana," *International Journal of Corrosion*, vol. 2014, 2014, Art. no. 679192, doi: 10.1155/2014/679192.

[38] T. Vennila and P. Manjula, "Corrosion inhibition, Adsorption behaviour and thermokinetic characteristics of 1-Benzyl-3-Hydroxy-1-H-Indazole on mildsteel in neutral medium," *Indian Journal of Applied Research*, vol. 6, no. 6, Jun. 2016.

[39] H. Baeza, M. Guzmán, P. Ortega, and L. Vera, "Corrosion inhibition of copper in 0.5 m hydrochloric acid by 1,3,4-Thiadiazole-2,5-Dithiol," *Journal of the Chilean Chemical Society*, vol. 48, no. 3, pp. 23–26, 2003, doi: 10.4067/S0717-97072003000300004.

[40] M. E. Bakri, R. Touir, A. Tazouti, N. Dkhireche, M. E. Touhami, A. Rochdi, and A. Zarrouk, "Corrosion inhibition study of brass in simulated cooling water by triazole derivatives, cetyltrimethylammonium bromide and their mixture," *Arabian Journal for Science and Engineering*, vol. 41, no. 1, pp. 75–88, 2016, doi: 10.1007/s13369-014-1532-6.

[41] A. El-Sherbini, B. Khalil, C. Ismail, and D. Tobar, "The corrosion of copper metal in hcl solutions and the effect of molybdate and chromate," in *The International Conference on Aerospace Sciences and Aviation Technology*, vol. 16, pp. 1–9, May 2015, doi: 10.21608/asat.2015.22941.

[42] Q. Liu, H. Luo, C. F. Dong, K. Xiao, and X. G. Li, "The electrochemical behaviour of brass in $NaHSO_3$ solution without and with Cl-," *International Journal of Electrochemical Science*, vol. 7, pp. 11123–11136, 2012.

[43] A. K. Satpati and A. V. R. Reddy, "Electrochemical study on corrosion inhibition of copper in hydrochloric acid medium and the rotating ring-disc voltammetry for studying the dissolution," I*nternational Journal of Electrochemistry*, vol. 2011, pp. 1–8, 2011, doi: 10.4061/2011/173462.

[44] M. A. Quraishi, E. E. Ebenso, and M. Natesan, "Inhibition of atmospheric corrosion of mild steel by new green inhibitors under vapour phase condition," *International Journal of Electrochemical Science*, vol. 7, no. 8, pp. 7463–7475, 2012, doi: 10.1016/S1452-3981(23)15797-X.

[45] T. Ramdé, S. Rossi, and L. Bonou, "Corrosion inhibition action of sulfamethoxazole for brass in acidic media," *International Journal of Electrochemical Science*, vol. 11, no. 8, pp. 6819–6829, 2016, doi: 10.20964/2016.08.39.

[46] R. T. Loto, C. A. Loto, and A. P. Popoola, "Inhibition effect of deanol on mild steel corrosion in dilute sulphuric acid," *South African Journal of Chemistry*, vol. 68, pp. 105–114, 2015, doi: 10.17159/0379-4350/2015/v68a16.

[47] N. Wei, Y. Jiang, Z. Liu, Y. Ying, X. Guo, Y. Wu, Y. Wen, and H. Yang, "4-Phenylpyrimidine monolayer protection of a copper surface from salt corrosion," *RSC Advances*, vol. 8, no. 14, pp. 7340–7349, 2018, doi: 10.1039/C7RA12256J.

[51] L. A. Al Juhaiman, A. A. Mustafa, and W. K. Mekhamer, "Polyvinyl pyrrolidone as a green corrosion inhibitor of carbon steel in neutral solutions containing NaCl : Electrochemical and thermodynamic study," *International Journal of Electrochemical Science*, vol. 7, no. 9, pp. 8578–8596, 2012, doi: 10.1016/S1452-3981(23)18017-5.

[52] J. Basumatary, "Cavitation erosion-corrosion in marine propeller materials," Ph.D. dissertation, Faculty of Engineering and the Environment, University of Southampton, Southampton, England, 2017.

[53] N. Devi and J. Sarma, "Blood compatible hydrogel composed of starch, 2-acrylamido-2-ethylpropane sulfonic acid and acrylamide," *International Journal of Latest Research in Science and Technology*, vol. 3, no. 4, pp. 205–210, 2014.

[54] M. Shaban, E. S. H. El Ashry, H. Abdel-Hamid, A. Morsy, and S. Kandil, "Anti-biofouling of 2-acrylamido-2-methylpropane sulfonic acid grafted cellulose acetate membranes used for water desalination," *Chemical Engineering and Processing - Process Intensification*, vol. 149, 2020, Art. no. 107857, doi: 10.1016/j.cep.2020.107857.

[55] N. S. Al-Kadhi, A. E. Fotouh, Y. H. Kotp, F. A. Saad, R. K. Shah, and S. M. E. Rayes, "Utilization of polyvinylpyrrolidone as an organic template for the facile synthesis of

analcime nanoparticles for efficient removal of Pb(II) and Cu(II) ions from aqueous media," *Silicon*, vol. 16, no. 3, pp. 1387–1406, 2024, doi: 10.1007/s12633-023-02765-0.

[56] W.-T. Kim, D.-C. Park, W.-H. Yang, C.-H. Cho, and W.-Y. Choi, "Effects of electrospinning parameters on the microstructure of PVP/TiO_2 nanofibers," *Nanomaterials*, vol. 11, no. 6, Art. no. 1616, 2021. doi: 10.3390/nano11061616.

[57] S. Huang, Y. Liu, Y. Zhou, Q. Li, G. Ren, Q. Jing, and F. Ren, "Exploring the effect of PVP on the spherical agglomeration process and micromeritic properties of ascorbic acid," *Powder Technology*, vol. 342, pp. 929–937, 2019, doi: 10.1016/j.powtec.2018.09.039.

[58] M. Wittmann, K. Henze, K. Yan, V. Sharma, and J. Simmchen, "Rod-shaped microparticles — an overview of synthesis and properties," *Colloid and Polymer Science*, vol. 301, no. 7, pp. 783–799, 2023, doi: 10.1007/s00396-023-05111-3.

[59] P. L. Krapivsky and E. Ben-Naim, "Collective properties of adsorption–desorption processes," *The Journal of Chemical Physics*, vol. 100, no. 9, pp. 6778–6782, May 1994, doi: 10.1063/1.467037.

[60] K. Dreisewerd, "The desorption process in MALDI," *Chemical Reviews*, vol. 103, no. 2, 2003, doi: 10.1021/cr010375i.

[61] W. Yang, Z. Liu, and H. Huang, "Galvanic corrosion behavior between AZ91D magnesium alloy and copper in distilled water," *Corrosion Science*, vol. 188, 2021, Art. no. 109562, doi: 10.1016/j.corsci.2021.109562.

[62] A. S. Ismail, "Corrosion behavior of aluminum-silicon-copper-manganese alloy in sulfuric acid medium," *Silicon*, vol. 8, no. 2, pp. 211–216, 2016, doi: 10.1007/s12633-014-9226-y.

[63] L. You-You, C. Tie-Shan, W. Dong-Ying, Z. Jie, B. Cui-Min, S. Yi-kun, M. Xian-Ming, and C. Cong-Qian, "Electrochemical corrosion of FV520B stainless steel in solutions bearing hydrogen bromide and acetic acid at high temperature from 130 to 200 °C," *Corrosion Engineering, Science and Technology*, vol. 56, no. 7, pp. 639–647, Oct. 2021, doi: 10.1080/1478422X.2021.1933309.

[64] A. Dąbrowski, "Adsorption — from theory to practice," *Advances in Colloid and Interface Science*, vol. 93, no. 1, pp. 135–224, 2001, doi: 10.1016/S0001-8686(00)00082-8.

[65] A. Kuroki, M. Hiroto, Y. Urushihara, T. Horikawa, K. I. Sotowa, and J. R. Alcántara Avila, "Adsorption mechanism of metal ions on activated carbon," *Adsorption*, vol. 25, no. 6, pp. 1251–1258, 2019, doi: 10.1007/s10450-019-00069-7.